Silesian J. Pure Appl. Math.
vol. 6, is. 1 (2016), 97–110

Ferdinand Evert UILHOORN

Gas Engineering Group, Warsaw University of Technology, Poland

ESTIMATING RAPID FLOW TRANSIENTS USING EXTENDED KALMAN FILTER

Abstract. Theoretical and numerical modeling of flow transients in pipelines is a challenging field of research. The governing flow equations constitute a system of nonlinear hyperbolic partial differential equations enforcing the conservation laws for mass, momentum and energy. The application of these mathematical models might be limited due to the absence of complete knowledge about the physical phenomena and uncertainties. Information about the initial and boundary conditions is usually obtained from measurements. The presence of noise and inaccuracies, as well as inexactness of the flow model and numerical approximations for solving the full model can lead to predictions that differ from reality. In this paper, we deal with the problem of extracting information about states of the system in real time given noisy measurements. We solved the isothermal flow model during a hydraulic shock while using the extended Kalman filter to estimate the hidden state variables. To avoid spurious oscillations in the solution, the flow model in conservative form was solved using Roe's flux limiter within the finite volume framework to ensure the total variation diminishing property. Numerical approximation of the Jacobian was done with an adaptive routine and showed that most entries in the matrix are zero and therefore sparse. The robustness of the extended Kalman filter was examined by varying the noise statistics. In most of the situations, we can conclude that the extended Kalman filter was successful in estimating the rapid transients of natural gas.

2010 Mathematics Subject Classification: 93E11, 76N15.
Keywords: hydraulic shock, extended Kalman filter, finite volume method.
Corresponding author: F.E. Uilhoorn (frits.uilhoorn@is.pw.edu.pl).
Received: 20.06.2016.

1. Introduction

Mathematical modeling of flow transients in pipelines is a challenging research area. The governing equations constitute a system of nonlinear hyperbolic partial differential equations (PDEs) enforcing the conservation laws for mass, momentum and energy. Several authors [1, 2, 8, 9, 13] have simulated the behavior of natural gas under transient conditions.

The application of these mathematical models might be limited due to the absence of complete knowledge about the physical phenomena and uncertainties. Noise and inaccuracies in measurements, as well as model inexactness and numerical errors, can lead to results that substantially differ from the reality. More accurate models increase computational complexity that may limit its applicability, particularly for real-time estimation.

When the stochastic dynamical system is linear with additive Gaussian noises, the optimal solution is found by the well-known Kalman filter (KF) [11]. Although, attempts were made to use the KF for state estimation applied to flow models [4,16, 19,23], the filter is intractable for such nonlinear systems. For this reason, different approximate nonlinear filtering algorithms were developed, whereas the extended Kalman filter (EKF) [5, 10, 15] is one of the most popular filters. A complete overview of recursive Bayesian estimators can be found in [3].

In this work, the flow transients were estimated using the EKF during a severe condition, namely a rapid valve closure at the end of the pipeline. We evaluate the filter on estimation accuracy, robustness and computation time.

2. Fluid flow model

The flow transients in pipelines are described by a set of hyperbolic PDEs, which are derived from the conservation laws and expressed as follows [21]:

$$\frac{\partial \rho}{\partial t} + \frac{\partial}{\partial x}(\rho v) = 0, \tag{1}$$

$$\frac{\partial (\rho v)}{\partial t} + \frac{\partial (\rho v^2 + p)}{\partial x} = -\frac{w}{A} - \rho g \sin \alpha, \tag{2}$$

$$\rho \left(\frac{\partial h}{\partial t} + v \frac{\partial h}{\partial x} \right) - \frac{\partial p}{\partial t} - v \frac{\partial p}{\partial x} = \frac{\Omega + wv}{A}, \tag{3}$$

within domain $D = \{(x,t) : x \in [0,L], t \in [0,t_f]\}$ where L and t_f denote the pipeline length and final simulation time, respectively. Other variables and parameters are density ρ, velocity v, pressure p, frictional force w, cross-sectional area A, gravitational acceleration g, angle of inclination α, enthalpy h and heat flow into the pipe Ω. The independent variables x and t represent the spatial and time coordinates, respectively.

In line with Kiuchi [13] we assumed an isothermal flow field and ignored the convective term in equation (2) because it is small compared to the other terms. If we assume that compressibility factor z and temperature T are constant, then for the equation of state we write

$$\frac{p}{\rho} = zRT = a_s^2, \tag{4}$$

with constant wave speed a_s and specific gas constant R. Using the expression for the mass flow rate $\dot{m} = \rho v A$, the equations (1) and (2) for the simplified one-dimensional, isothermal flow model yield

$$\frac{\partial p}{\partial t} + \frac{a_s^2}{A}\frac{\partial \dot{m}}{\partial x} = 0, \tag{5}$$

$$\frac{\partial \dot{m}}{\partial t} + A\frac{\partial p}{\partial x} + \frac{f a_s^2}{2dA}\frac{\dot{m}\,|\dot{m}|}{p} = 0. \tag{6}$$

with friction factor f and pipe diameter d.

Equations (5) and (6) are convenient to work with in engineering practice. For more accurate predictions, the energy equation (3) should be included [1, 2]. However, improving the model accuracy results in higher computation times that might make it less applicable to real-time estimation. Uncertainties in flow modeling are related to changes in natural gas composition, roughness factor [14], surrounding temperature along the pipeline and burial depth [8, 9]. For buried pipelines, soil properties such as heat capacity, thermal conductivity and diffusivity of the soil change over time as it alternately wets and dries. These quantities are difficult to determine. Even if we have a perfect flow model, the information about the initial and boundary conditions is not perfect. Thus, results will not be in agreement with reality.

In this work, we approach the state variables p and $\dot{m}$ as realizations of a stochastic process whereas the most likely state can be extracted from the probability density function (pdf). We have an approximated flow model with uncertain estimates of model parameters, initial and boundary conditions and on the other

hand, we have noisy measurements. Mathematically, the evolution of the state sequence $\{\mathbf{x}_k, k \in \mathbb{N}\}$ can be written as follows:

$$\mathbf{x}_k = f(\mathbf{x}_{k-1}) + \mathbf{v}_{k-1}, \tag{7}$$

where the aim is to estimate $\mathbf{x}_k$ from measurements,

$$\mathbf{y}_k = h(\mathbf{x}_k) + \mathbf{n}_k, \tag{8}$$

where f and h represent the flow and measurement model, respectively. In the stochastic state space model $\mathbf{v}_{k-1}$ is a random vector that captures uncertainties in the flow model and $\mathbf{n}_k$ denotes the measurement noise. In the EKF both are mutually independent with normal probability distributions, $\mathbf{v}_{k-1} \sim \mathcal{N}(0, \mathbf{Q}_{k-1})$ and $\mathbf{n}_k \sim \mathcal{N}(0, \mathbf{R}_k)$ with covariances $\mathbf{Q}_{k-1}$ and $\mathbf{R}_k$, respectively. The state vector $\mathbf{x}_k$ refers to system variables p and $\dot{m}$.

3. Numerical solution

The isothermal flow model was solved with a high-resolution finite volume scheme using Roe's superbee flux limiter [17]. High resolution schemes try to suppress numerical dissipation and unwanted oscillations due to shocks or steep gradients in the solution domain. Flux limiters ensure the total variation diminishing (TVD) property [7] at which the local under- and overshoot is avoided. First, we formulate the set of equations in compact form as follows:

$$\frac{\partial \mathbf{u}}{\partial t} + \frac{\partial \mathbf{f}(\mathbf{u})}{\partial x} = \mathcal{S}(\mathbf{u}), \tag{9}$$

with

$$\mathbf{u}\,(x,t) = \mathbf{u} = \begin{bmatrix} p \\ \dot{m} \end{bmatrix}, \quad \mathbf{f}\,(\mathbf{u}) = \begin{bmatrix} \frac{a_s^2}{A}\dot{m} \\ Ap \end{bmatrix}, \quad \mathcal{S}\,(\mathbf{u}) = \begin{bmatrix} 0 \\ -\frac{f a_s^2}{2dA}\frac{\dot{m}|\dot{m}|}{p} \end{bmatrix}. \tag{10}$$

Within the finite volume framework, we divide the interval $[0, L]$ in cells defined by I_i=$[x_{i-1/2}, x_{i+1/2}]$, $i \in \mathbb{Z}$ where $x_i = (x_{i+1/2}, x_{i-1/2})/2$ is the midpoint of I_i. Let $\Delta x_i = x_{i+1/2} - x_{i-1/2}$ be the mesh size, $\Delta x_{i+1/2} = x_{i+1} - x_i$. The mesh is fixed in time. Integration of (9) over I_i yields

$$\frac{\mathrm{d}}{\mathrm{d}t}u_i(t) + \frac{1}{\Delta x_i}(f(u(x_{i+1/2},t)) - f(u(x_{i-1/2},t))) = \frac{1}{\Delta x_i}\int\limits_{I_i}\mathcal{S}(u(x,t))\,\mathrm{d}x, \quad (11)$$

Let u_i be the cell average of u on I_i, then we read

$$u_i(t) = \frac{1}{\Delta x_i}\int\limits_{i-1/2}^{i+1/2} u(x,t)\,\mathrm{d}x. \quad (12)$$

Defining χ_{I_i} as the characteristic function of cell I_i, we aim to find a piecewise constant function,

$$u_u(x,t) = \sum_{i\in\mathbb{Z}} U_i(t)\chi_{I_i}(x), \quad (13)$$

with

$$\frac{\mathrm{d}}{\mathrm{d}t}U_i(t) + \frac{1}{\Delta x_i}(\mathcal{F}_{i+1/2} - \mathcal{F}_{i-1/2}) = \mathcal{S}_i, \quad (14)$$

$$U_i(0) = \frac{1}{\Delta x_i}\int\limits_{i-1/2}^{i+1/2} u(x,0)\,\mathrm{d}x, \quad (15)$$

where $\mathcal{F}_{i+1/2} = \mathcal{F}(U^-_{i+1/2}, U^+_{i+1/2})$ is the monotone numerical flux that approximates $f(u(x_{i+1/2},t))$. The source $\mathcal{S}_i$ is calculated from the expression

$$\mathcal{S}_i = \mathcal{S}_i(U_i) \approx \frac{1}{\Delta x_i}\int\limits_{i-1/2}^{i+1/2}\mathcal{S}(u(x,t))\,\mathrm{d}x \quad (16)$$

The approximations $U^-_{i+1/2}, U^+_{i+1/2}$ of the point value $u(x_{1+1/2},t)$ of I_i and I_{i+1} are obtained via a reconstruction process. For our purpose, the classical MUSCL (Monotonic Upstream-Centered Scheme for Conservation Laws) linear reconstruction [22] is applied. It assumes a piecewise-linear interpolation from the average values. The reconstruction for each component can be defined as

$$U^-_{i+1/2} = U_i + \frac{1}{2}\phi(\theta_i)(U_{i+1} - U_i), \quad (17)$$

and

$$U^+_{i+1/2} = U_{i+1} - \frac{1}{2}\phi(\theta_i)(U_{i+2} - U_{i+1}), \quad (18)$$

where θ is

$$\theta_i = \frac{U_i - U_{i-1}}{U_{i+1} - U_i}, \quad (19)$$

and ϕ is a slope limiter function [20] that limits the slope of the piecewise approximations to ensure TVD and avoid spurious oscillations that would otherwise occur around discontinuities or shocks. In this scheme, numerical dissipation is minimized when $\phi(\theta)$ increases. Its resolution is higher at the discontinuities or shocks. On the other hand, more dissipation from the limiter is expected when $\phi(\theta)$ decreases. It has a lower resolution. In this work, we used Roe's superbee flux limiter [17] because it is considered as a good compromise between accuracy and computational efficiency [6]. This limiter is given as follows:

$$\phi(\theta) = \max(0, \min(2\theta, 1), \min(\theta, 2)), \quad \lim_{\theta \to \infty} \phi(\theta) = 2. \tag{20}$$

The finite volume discretization of the source term is done as follows:

$$\frac{1}{\Delta x} \int_{I_i} \mathcal{S} \, \mathrm{d}x \approx \frac{\mathcal{S}_{i-1/2} + \mathcal{S}_{i+1/2}}{2}, \tag{21}$$

where

$$\mathcal{S}_{i+1/2} = \mathcal{S}\left(\frac{U^-_{i+1/2} + U^+_{i+1/2}}{2} \right). \tag{22}$$

In order to solve the time-dependent problem the resulting spatially discretized equations must be integrated in time. This is done with the classical fourth-order Runge-Kutta method.

4. Extended Kalman filter

The most used estimator for nonlinear systems is probably the extended Kalman filter because of its simplicity, robustness and suitability for real-time implementations. It approximates the optimal estimate based on linearization of both process and measurement model. Below we give a brief overview, the more theoretical considerations are described in [5, 10, 15].

The process model we use is our flow model (9), whereas the state vector is defined by pressure and mass flow rate. At time step $k-1$, the prediction step is performed by finding the a priori state estimate $\hat{\mathbf{x}}_{k|k-1}$ via integration using the Runge-Kutta scheme. Next, the a priori estimate of the error covariance is written as

$$\mathbf{P}_{k|k-1} = \mathbf{F}_k \mathbf{P}_{k-1|k-1} \mathbf{F}_k^\top + \mathbf{Q}_{k-1}, \tag{23}$$

where $\mathbf{Q}_{k-1}$ is the covariance of the process noise, $\mathbf{P}_{k-1|k-1}$ is the a posteriori estimate of the error covariance and matrix $\mathbf{F}_k$ contains the partial derivative elements of the Jacobian that is calculated as follows:

$$\mathbf{F}_{k,[i,j]} = \left.\frac{\partial f_i}{\partial x_j}\right|_{(\hat{\mathbf{x}}_{k-1|k-1})}. \tag{24}$$

where f represents the flow model. Given the covariance matrix $\mathbf{R}_k$ of the measurement noise, the correction step calculates the a posteriori state estimate via

$$\hat{\mathbf{x}}_{k|k} = \hat{\mathbf{x}}_{k|k-1} + \mathbf{K}_k(\mathbf{y}_k - \mathbf{H}_k\hat{\mathbf{x}}_{k|k-1}), \tag{25}$$

where $\mathbf{K}_k$ is the Kalman gain and $\mathbf{H}_k$ is the measurement matrix. The Kalman gain reads

$$\mathbf{K}_k = \mathbf{P}_{k|k-1}\mathbf{H}_k^\top(\mathbf{H}_k\mathbf{P}_{k|k-1}\mathbf{H}_k^\top + \mathbf{R}_k)^{-1}, \tag{26}$$

and the elements of the measurement matrix as

$$\mathbf{H}_{k,[i,j]} = \left.\frac{\partial h_i}{\partial x_j}\right|_{(\hat{\mathbf{x}}_{k-1|k-1})}. \tag{27}$$

At the end we compute the a posteriori estimate of the error covariance, which is defined by

$$\mathbf{P}_{k|k} = \mathbf{P}_{k|k-1} - \mathbf{K}_k\mathbf{H}_k\mathbf{P}_{k|k-1}. \tag{28}$$

When the state variables are directly available, the Jacobian is equal to the identity matrix. The Jacobian of the flow model is computed with the adaptive-routine called `numjac` coded in Matlab and developed by Salane [18] for the approximation of partial derivatives when integrating a system of ODEs. For large ODE systems, most entries in the matrix are zero and therefore sparse.

5. Numerical experiments

Numerical experiments were conducted to examine the estimation accuracy, robustness and computation time of the EKF. The first measure in terms of root mean square error (RMSE) is defined as

$$\mathrm{RMSE} = \frac{1}{\tau}\sum_{j=1}^{\tau}\left(\frac{\|\mathbf{X}-\hat{\mathbf{X}}\|_F}{\sqrt{N_d N_k}}\right), \tag{29}$$

where τ is the number of Monte Carlo runs, $\mathbf{X}$ is the true and $\hat{\mathbf{X}}$ is the estimated matrix representing p and $\dot{m}$ within domain D. The number of nodes and time steps are denoted as N_d and N_k, respectively. The state estimates are compared with the true values, which are the numerical solution with additive Gaussian random noise.

The robustness of the EKF was examined by varying the noise statistics. The CPU time was measured using Matlab's built-in `tic-toc` dual function and averaged over τ runs. Simulations have been performed on a PC with an Intel(R) Core(TM) i3-2348M 2.30 GHz, 8 GB RAM, Windows 7 64-bit. The numerical approximations of the PDE system together with the EKF were written in Matlab R2014a 64-bit.

The state variables pressure and mass flow rate were estimated during a hydraulic shock. The system was characterized by a pipeline length of 20 km and internal diameter of 0.5 m. The friction factor was assumed to be 0.008. The natural gas density under normal conditions is 0.856 $\mathrm{kg\,m^{-3}}$ with a compressibility factor of 0.9. The boundary conditions were set to $p(0,t) = 5.0$ MPa and $\dot{m}(L,t)$ is shown in Figure 1.

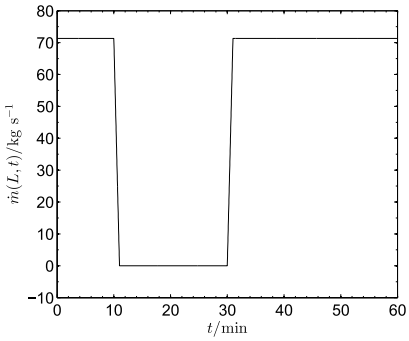

Fig. 1. Mass flow rate boundary condition

After 10 min the valve at the outlet node was closed for 20 min and opened again, whereas the gas flow increased from zero to 71.3 $\mathrm{kg\,s^{-1}}$. We assumed that the valve closed linearly within 60 s. To avoid inverse crime [12], the solutions were first obtained using a finer step size of the grid $\Delta x = 100$ m and time step $\Delta t = 0.25$ s for the integration. The size of Jacobian matrix for the fine resolution

model was 402×402 with 1200 nonzero elements and for the coarse model we obtained a 102×102 matrix with 300 nonzero elements. The reduced model solution was obtained using $\Delta x = 400$ m and $\Delta t = 1$ s with a CPU time of 14.6 s.

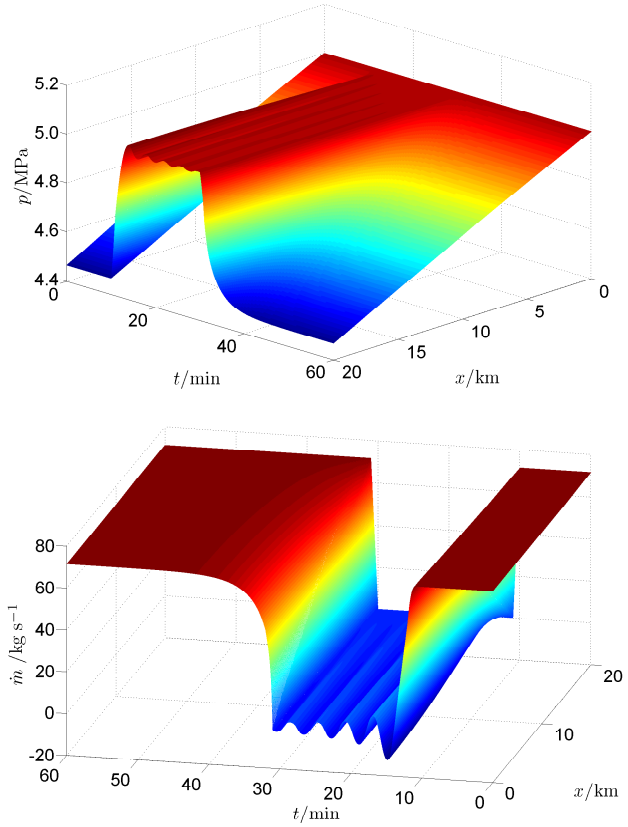

Fig. 2. Spatial-temporal evolution of pressure and mass flow rate without noise

Figure 2 shows the evolution of pressure and mass flow rate without model noise. The CPU time for the solution with fine resolution grid spacing was 231.7 s. When the valve was closed, the natural gas adjacent to the valve was brought to rest. As a consequence, it propagated a pressure and flow rate wave backward. The reverse flow decreased the pressure and caused oscillations in pressure and flow. The maximum estimated values during the oscillation were 7.522 $\mathrm{kg\,s^{-1}}$ and 5.005 MPa, while the minimum values were -11.676 $\mathrm{kg\,s^{-1}}$ and 4.993 MPa. The frictional dissipation damped out the oscillation. Although, flux limiters aim to

obviate numerical dissipation in the solution, its existence can lead to erroneous estimation of the amplitudes of the pressure and flow rate waves.

The measurements were obtained by adding to the fine grid solution a Gaussian random noise of $\mathcal{N}\left(n_k; 0, 0.05^2\right)$ and $\mathcal{N}\left(n_k; 0, 1^2\right)$ with variance in MPa^2 and $(\mathrm{kg\,s^{-1}})^2$, respectively. The standard deviation of the model noise for pressure $\sigma_{v_k,p}$ and mass flow rate $\sigma_{v_k,\dot{m}}$ was set to 0.055 MPa and 1.1 $\mathrm{kg\,s^{-1}}$, respectively. It was assumed 10% higher than that of the measurement noise ($\sigma_{n_k,p} = 0.05$ MPa and $\sigma_{n_k,\dot{m}} = 1\ \mathrm{kg\,s^{-1}}$). We conducted 20 simulation runs ($\tau = 20$) with different initial realizations.

The initialization of the EKF was done by setting $\partial\mathbf{h}/\partial t$ in (9) equal to zero. The a priori estimate of the error covariance matrix was set equal to the identity matrix. The off-diagonal entries of $\mathbf{Q}$ and $\mathbf{R}$ were zero and the diagonal entries correspond to the process and measurement noise covariance, that is, $\sigma^2_{v_k}$ and $\sigma^2_{n_k}$, respectively. The results of the EKF are illustrated in Figure 3.

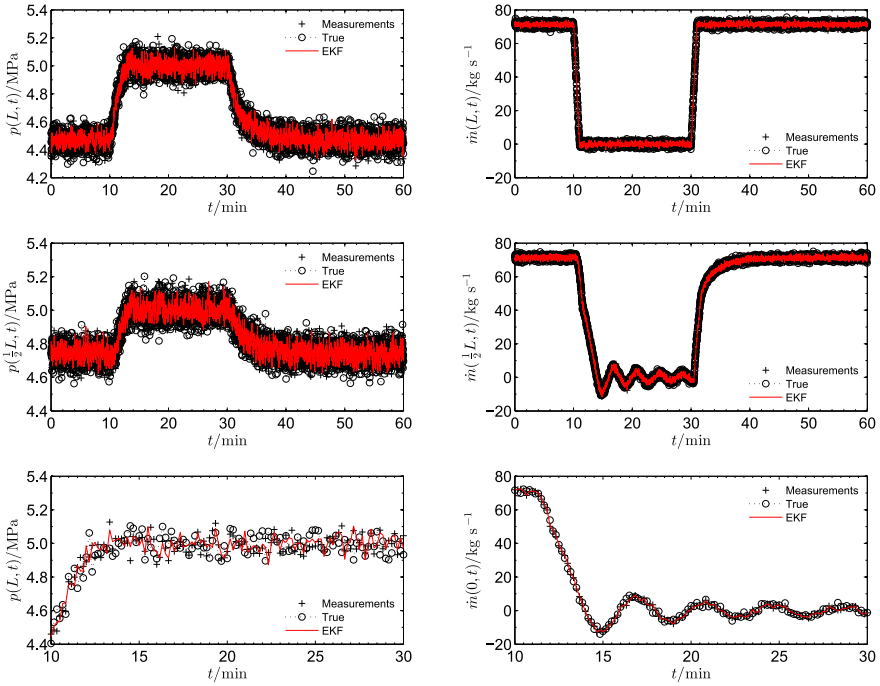

Fig. 3. Measurements, true and estimates of pressure and mass flow rate; $\sigma_{v_k} = 1.1 \cdot \sigma_{n_k}$ where $\sigma_{n_k,p} = 0.05$ MPa and $\sigma_{n_k,\dot{m}} = 1\ \mathrm{kg\,s^{-1}}$

To test the robustness of the EKF we examined different noise statistics by varying the standard deviation of the model noise σ_{v_k} and measurement noise σ_{n_k}. Besides this, the RMSE, its $\pm$ 1 standard error (SE) over τ simulations with different realizations and mean CPU time $\bar{t}_{cpu}$ were calculated. First, we kept σ_{n_k} constant and varied σ_{v_k}. Table 1 shows that the standard deviation of the model noise impacts the performance of the filter. Higher values for the process noise result in a higher Kalman gain (26) meaning that more measurement information is included to adjust the predicted state variables p and $\dot{m}$. Thus, we trust the measurements more than the model. In case of a too low value for the process noise, the EKF might fail to converge because it depends too much on our inexact flow model and too less on measurements. This situation occurred for $\sigma_{v_k} = 0.1 \cdot \sigma_{n_k}$ as we see in Table 1 and Figure 4. Moreover, the higher SE over τ runs for both state variables indicated that the random changes become more significant. Between $t \in [10, 30]$ we can see that the filter tries to recover and seems to perform better for the pressure estimates. This might be a result of having a lower degree of nonlinearity in the pressure waves compared to the mass flow rate. The latter showed a lag behind the actual values. Non-convergence for both state variables was resolved when we added more uncertainty regarding our knowledge about the pressure. When we increased it only for the mass flow rate, the filter still failed for the pressure estimates. This implies that the uncertainty associated with the pressure is an important tuning parameter in the EKF for the flow model. In Table 2 we kept σ_{v_k} constant and varied σ_{n_k}. If we increase the measurement noise, the Kalman gain gets smaller, thus we trust more the flow model. The filter did not show convergence problems for the selected noise statistics in Table 2.

Table 1
RMSE, SE and $\overline{t}_{\mathrm{cpu}}$ for different standard deviations of model noise; $\sigma_{n_{k,p}} = 0.05$ MPa and $\sigma_{n_{k,\dot{m}}} = 1\ \mathrm{kg\,s^{-1}}$

$\sigma_{v_k} =$	$1.9 \cdot \sigma_{n_k}$	$1.1 \cdot \sigma_{n_k}$	$0.9 \cdot \sigma_{n_k}$	$0.1 \cdot \sigma_{n_k}$
$\mathrm{RMSE}_p/10^{-1}\mathrm{MPa}$	1.053	0.689	0.603	0.501
$\mathrm{SE}/10^{-4}\mathrm{MPa}$	0.471	0.241	0.240	2.650
$\mathrm{RMSE}_{\dot{m}}/\mathrm{kg\,s^{-1}}$	2.143	1.479	1.337	6.066
$\mathrm{SE}/10^{-3}\mathrm{kg\,s^{-1}}$	0.725	0.396	0.548	2.631
$\overline{t}_{\mathrm{cpu}}/\mathrm{s}$	291.8	289.7	260.7	257.1

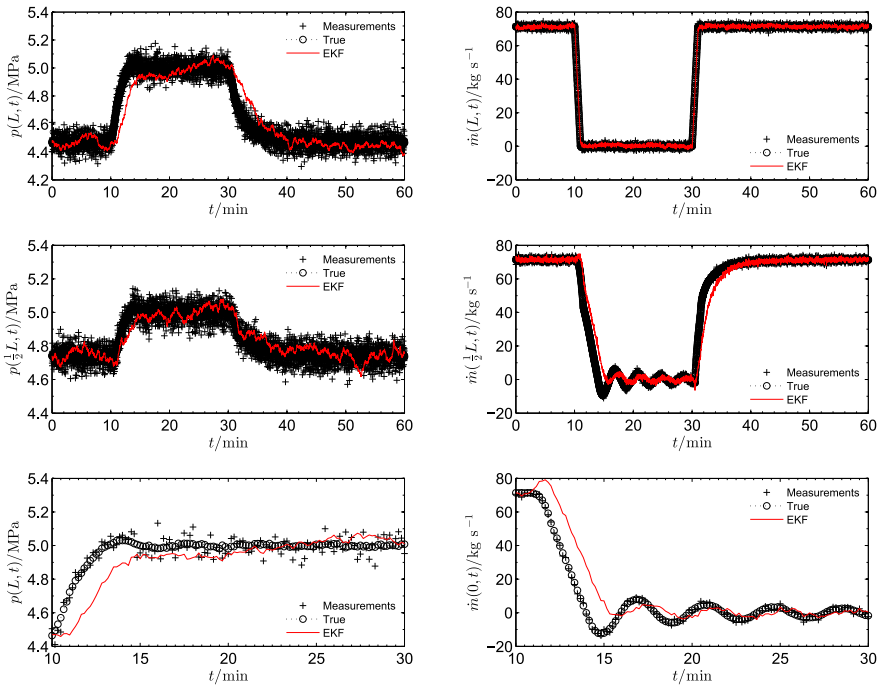

Fig. 4. Measurements, true and estimates of pressure and mass flow rate; $\sigma_{v_k} = 0.1 \cdot \sigma_{n_k}$ where $\sigma_{n_k,p} = 0.05$ MPa and $\sigma_{n_k,\dot{m}} = 1$ kg s^{-1}

Table 2
RMSE, SE and $\overline{t}_{\text{cpu}}$ for different standard deviations of measurement noise; $\sigma_{v_{k,p}} = 0.055$ MPa and $\sigma_{v_{k,\dot{m}}} = 1.1$ kg s^{-1}

$\sigma_{n_k} =$	$1.9 \cdot \sigma_{v_k}$	$1.1 \cdot \sigma_{v_k}$	$0.9 \cdot \sigma_{v_k}$	$0.1 \cdot \sigma_{v_k}$
RMSE$_p$/10^{-2}MPa	8.678	6.671	6.246	5.027
SE/10^{-5}MPa	4.602	2.529	2.401	1.228
RMSE$_{\dot{m}}$/kg s^{-1}	2.123	1.478	1.340	1.005
SE/10^{-4}kg s^{-1}	6.274	5.843	3.889	2.631
$\overline{t}_{\text{cpu}}$/s	246.5	256.0	259.6	260.4

6. Conclusion

In this paper, we investigated the performance of the EKF applied to hyperbolic flow model to estimate the transients during a hydraulic shock. In general, we can conclude that EKF is in most of the situations successful. Limitations

emerge when we operate in the low model noise domain, the filter might show convergence problems. In this situation, it relies too much on the inexact flow model and too less on measurements. Especially, model uncertainty associated with the pressure state variable seems to be an important tuning parameter in the EKF.

Further research should be focused on the role of numerical dissipation and investigating different system configurations. Simulated data based on more accurate flow models would be interesting, instead of introducing more uncertainty in the simplified flow model as we did. Real data would be prefered.

References

1. Abbaspour M., Chapman K. S.: *Nonisothermal transient flow in natural gas pipeline*. ASME. J. Appl. Mech. **75**, no. 3 (2008), 031018–031018-8.
2. Chaczykowski M.: *Transient flow in natural gas pipeline – the effect of pipeline thermal model*. Appl. Math. Model. **34**, no. 4 (2009), 1051–1067.
3. Chen Z.: *Bayesian Filtering: From Kalman Filters to Particle Filters, and Beyond*. Technical report, Communications Research Laboratory, McMaster University, Canada 2003.
4. Durgut I., Leblebicioğlu K.: *Kalman-Filter observer design around optimal control policy for gas pipelines*. Internat. J. Numer. Methods Fluids **24**, no. 2 (1997), 233–245.
5. Gelb A.: *Applied Optimal Estimation*. MIT Press, Cambridge 1974.
6. Griffiths G., Schiesser W.: *Traveling Wave Analysis of Partial Differential Equations: Numerical and Analytical Methods with Matlab and Maple*. Academic Press, Amsterdam 2011.
7. Harten A.: *High resolution schemes for hyperbolic conservation laws*. J. Comput. Phys. **49**, no. 3 (1983), 357–393.
8. Helgaker J. F., Muller B., Ytrehus T.: *Transient flow in natural gas pipelines using implicit finite difference schemes*. ASME. J. Offshore Mech. Arct. Eng. **136**, no. 3 (2014), 031701–031701–11.
9. Helgaker J. F., Oosterkamp A., Langelandsvik L. I., Ytrehus T.: *Validation of 1D flow model for high pressure offshore natural gas pipelines*. J. Natural Gas Sci. Eng. **16** (2014), 44–56.
10. Jazwinski A.H.: *Stochastic Processes and Filtering Theory*. Academic Press, New York 1970.

11. Kalman R.E.: *A new approach to linear filtering and prediction problems.* Trans. ASME J. Basic Eng., Ser. D **82** (1960), 34–45.
12. Kaipio J., Somersalo E.: *Statistical inverse problems: discretization, model reduction and inverse crimes.* J. Comput. Appl. Math.**198**, no. 2 (2007), 493–504.
13. Kiuchi T.: *An implicit method for transient gas flows in pipe networks.* Int. J. Heat Fluid Flow **15**, no. 5 (1994), 378–383.
14. Langelandsvik L., Postvoll W., Aarhus B., Kaste K.: *Accurate calculation of pipeline transport capacity.* Proceedings to World Gas Conference 2009.
15. Maybeck P.S.: *Stochastic Models, Estimation and Control: Volume 1.* Academic Press, New York 1979.
16. Ozawa A., Sanada K.A.: *Kalman filter for estimating transient pressure and flow rate in a pipe.* In SICE Annual Conference, Japan 2011.
17. Roe P.L.: *Characteristic-based schemes for the Euler equations.* Annu. Rev. Fluid Mech. **18**, no. 1 (1986), 337–365.
18. Salane D.E.: *Adaptive Routines for Forming Jacobians Numerically.* Technical Report SAND86-1319, Sandia National Laboratories, 1986.
19. Sanada K.: *Using a Kalman Filter to Estimate Unsteady Flow.* Int. J. Autom. Tech. **6**, no. 4 (2012), 440–444.
20. Sweby P.K.: *High resolution schemes using flux limiters for hyperbolic conservation laws.* SIAM J. Numer. Anal. **21**, no. 5 (1984), 995–1011.
21. Thorley A.R.D., Tiley C.H.: *Unsteady and transient flow of compressible fluids in pipelines-a review of theoretical and some experimental studies.* Int. J. Heat Fluid Flow **8**, no. 1 (1987), 3–15.
22. Van Leer B.: *Towards the ultimate conservative difference scheme V. A second order sequel to Godunov's method.* J. Comput. Phys. **32** (1979), 101–136.
23. Vianna F.L.V., Orlande H.R.B., Dulikravich G.S.: *Estimation of the temperature field in pipelines by using the Kalman filter.* In 2nd International Congress of Serbian Society of Mechanics, Serbia 2009.